Directional photoelectric current across the bilayer graphene junction

2009 J. Phys.: Condens. Matter 21 015301

(http://iopscience.iop.org/0953-8984/21/1/015301)

J. Phys.: Condens. Matter **21** (2009) 015301 (7pp) doi:10.1088/0953-8984/21/1/015301

Directional photoelectric current across the bilayer graphene junction

S E Shafranjuk[1]

Department of Physics and Astronomy, Northwestern University, Evanston, IL 60208, USA

Received 8 September 2008, in final form 27 October 2008
Published 1 December 2008
Online at stacks.iop.org/JPhysCM/21/015301

Abstract
A directional photon-assisted resonant chiral tunneling through a bilayer graphene barrier is considered. An external electromagnetic field applied to the barrier switches the transparency T in the longitudinal direction from its steady state value $T = 0$ to the ideal $T = 1$ at no energy costs. The switch happens because the ac field affects the phase correlation between the electrons and holes inside the graphene barrier, changing the whole angular dependence of the chiral tunneling (directional photoelectric effect). The suggested phenomena can be implemented in relevant experiments and in various sub-millimeter and far-infrared optical electronic devices.

1. Introduction

The electromagnetic properties of bilayer graphene [1–4] offer enormous opportunities for scientific research and various nanoelectronic applications. They emerge in the spectroscopy of bound and scattering states, in the photon-assisted chiral tunneling and in direct probing of strong correlation effects. Potential applications include electromagnetic field (EF) spectral analyzers, receivers, detectors and sensors [5]. The crystal lattice of the bilayer graphene [1–4] consists of four equivalent sublattices of carbon atoms while the charge carriers behave there as massive 'chiral fermions' [1, 3, 4]. The chiral fermions (CF) in bilayer graphene have a finite mass $m_{e,h}$, like conventional electrons (e) and holes (h) in metals and semiconductors [1, 3, 4]. The chirality relates the particles to certain sublattices and is responsible for various unconventional dc electronic and magnetic properties of the bilayer graphene [1–3]. In contrast to an ordinary tunneling through a conventional potential barrier, during the chiral tunneling (CT) an incoming electron is converted into a hole moving inside the graphene barrier in a reverse direction, as indicated in figure 1(a) (the Klein paradox [7, 8]). This yields a finite transparency $\overline{T} \neq 0$ for incident electrons with energies E below the barrier $E < U_0$ (U_0 is the barrier height energy) occurring [1] at finite particle incidence angles $\phi \neq 0$. On the other hand, the steady state chiral tunneling is blocked ($\overline{T} = 0$) in the longitudinal direction $\phi = 0$. The angle-dependent transparency makes the chiral tunneling attractive for various nanoelectronic applications [5, 6]. The potential barrier in graphene can either be induced by the gate voltage V_G from a Si gate slab or can be formed by three overlapping graphene sheets, as shown in figures 1(c) and (d). According to [1], the dc gate voltage V_G shifts the graphene barrier height, which controls the chiral tunneling. That process

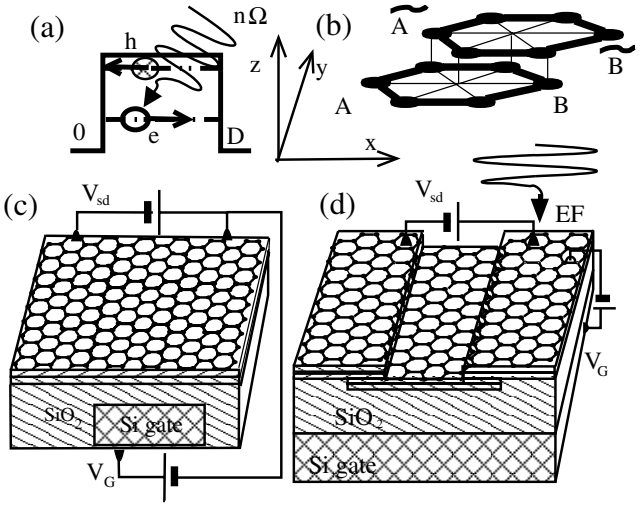

Figure 1. (a) Potential barrier in bilayer graphene controlled by the gate voltage V_G and exposed to the external electromagnetic field, EF. The scattering states inside the barrier originate from conversion of an electron (e) to a hole (h). (b) Two coupled hexagonal lattices with non-equivalent carbon atomic sites A, B, $\tilde{A}$, and $\tilde{B}$ in the bottom and top layers respectively. Two possible set-ups (c) and (d) of the bilayer graphene junction. The external ac field induces the directional photon-assisted resonant tunneling.

[1] URL: http://kyiv.phys.northwestern.edu

implies the wavefunction phases of electrons and holes being interconnected with each other in the graphene. The phase correlations during the chiral tunneling can also be directly tuned by applying an external ac field. Control of the electron wavefunction phase by an ac field has not been accomplished yet and is the subject of this paper. The electronic properties are described by a spinor wavefunction $\hat{\Psi}$, whose components depend on the angle ϕ between the electron momentum $\mathbf{p}$ and the x axis (see figure 1). A similar spinor description had formerly been used for Dirac fermions [7] and for relativistic quasiparticles in single-layer graphene [1, 9].

This paper is devoted to electromagnetic properties of a bilayer graphene junction shown in figure 1. One may expect that the differential tunneling conductance $\sigma(\phi, V_{\rm sd})$ of 'clean' samples depends on the angle ϕ between the electric current $\mathbf{j}$ and the x direction (see figure 1). The whole shape of $\sigma(\phi)$ versus the source–drain voltage $V_{\rm sd}$ is very sensitive to properties of the bilayer graphene barrier. We begin with computing the steady state $\sigma(\phi, V_{\rm sd})$ curves for a graphene barrier biased by $V_{\rm sd}$. The steady state results are then utilized for studying the ac properties. When an external electromagnetic field (EF) is applied, it strongly affects the directional diagram of $\sigma(\phi, V_{\rm sd})$. In particular we will see that the external electromagnetic field induces a finite conductance in the straightforward direction ($\phi = 0$), which had been blocked in the steady state. That happens because the electromagnetic field affects the electron–hole phase correlations inside the graphene barrier directly. In the steady state, when the ac field is off, the electric current is fully suppressed at $V_{\rm sd} < U_0$ (for a typical gate voltage $V_{\rm G} = 1$ V and SiO_2 thickness $d = 300$ nm one finds [9] $U_0 = 2$ meV).

2. Photon-assisted chiral tunneling

Here we examine the influence of an electromagnetic field on chiral tunneling and discuss the intrinsic noise. For studying the non-stationary electric current across the bilayer graphene junction we implement the methods of [10–12]. The graphene bilayer is modeled as two coupled hexagonal lattices consisting of four non-equivalent sites A, B and $\tilde{\rm A}$, $\tilde{\rm B}$ in the bottom and top layers respectively (see figure 1(a)). The chiral fermion Hamiltonian operates in the space of the two-component wavefunctions $\hat{\Psi}$. When the junction is exposed to an external electromagnetic field, the main part of the Hamiltonian is

$$\hat{H} = -\hbar^2 \left(\pi_-^2 \hat{\sigma}_+ + \pi_+^2 \hat{\sigma}_-\right)/2m + U(x), \qquad (1)$$

where $\pi_\pm = (k - eA_x(t)/\hbar) \pm {\rm i}(q - eA_y(t)/\hbar)$, $\hat{\sigma}_\pm = \hat{\sigma}_x \pm \hat{\sigma}_y$, $\hat{\sigma}_i$ are the Pauli matrices, $i = \{x, y, z\}$, the effective mass m is expressed via the coupling strength $\gamma_{\tilde{\rm A}\rm B}$ between $\tilde{\rm A}$ and B as $m = \gamma_{\tilde{\rm A}\rm B}/2v^2 = 0.054\, m_{\rm e}$, where $v = (\sqrt{3}/2)a\gamma_{\rm AB}$, $a = 0.246$ nm is the lattice constant, $\gamma_{\rm AB} \approx 0.4$ eV, $A_{x,y}(t)$ are the corresponding components of the time-dependent vector potential $\mathbf{A}(t)$ and $U(x)$ is the graphene barrier potential controlled by the gate voltage $V_{\rm G}$. Equation (1) describes interlayer coupling via a dimer state formed by pairs of carbon $\rm A\tilde{B}$ atoms located in the bottom and top layers, respectively, as shown in figure 1(b). A weak direct $\rm A\tilde{B}$ coupling and a small interaction due to the bottom and top layer asymmetry (which opens a minigap in the electron spectrum [3]) are both hereafter neglected.

For graphene junctions having finite dimensions, the motion of chiral fermions is quantized. The quantization imposes additional constraints on the directional tunneling diagram. Permitted values of the angle $\tilde{\phi}_n$ inside the graphene barrier are obtained from boundary conditions along the y direction, so the y component of the electron momentum $\mathbf{p} = (\hbar k, \hbar q)$ is quantized as $\tilde{q}_n = n\pi/W$ (where W is the barrier width), which gives $\tilde{\phi}_n = \arctan[n\pi/(k'_\varepsilon W)]$, where $k'_\varepsilon = \sqrt{2m/\hbar^2}\sqrt{|\varepsilon - U_0| - |\varepsilon|(1 - \cos 2\phi)/2}$. The last formula also means that $\tilde{q}_n$ depends on the electron energy variable ε. The electric current density $j = I(V_{\rm sd})/W$ (I is the electric current, $V_{\rm sd}$ is the bias voltage and W is the graphene stripe width) between electrodes 1 and 3 is computed as $j = 2\pi e \int {\rm d}\varepsilon\, \chi_\varepsilon [G_3^K(\varepsilon) - G_1^K(\varepsilon)]$ where we introduced the factor χ_ε. If electrodes 1 and 3 are made of a monolayer graphene or are metallic, then $\chi_\varepsilon = v_{\rm F} N(0)$, where $v_{\rm F}$ and $N(0)$ are corresponding Fermi velocity and the electron density of states at the Fermi level. However, if electrodes 1 and 3 are made of the bilayer graphene itself, which case we inspect in detail below, then $\chi_\varepsilon = v_\varepsilon N(\varepsilon)$, where $v_\varepsilon = \hbar|k|/m = \sqrt{2|\varepsilon|/m}$ and $N(\varepsilon) = \sum_k \theta(\varepsilon - E_k) \cdot m/(\pi\hbar^2)$ are the energy-dependent velocity and the two-dimensional electron density of states in the bilayer graphene, E_k is the kth electron energy level in the graphene barrier stripe, $G_r^K(\varepsilon) = -{\rm i}\sum_p |t_p|^2 {\rm e}^{{\rm i}q_y} {\rm e}^{{\rm i}kD}(2n_p - 1)\delta(\varepsilon - \varepsilon_p + \delta_{r,3} eV_{\rm sd})$ is the Keldysh Green function [11], r is the electrode index, $\delta_{r,3}$ is the Kronecker symbol and n_p is the distribution function of electrons with momentum $\mathbf{p}$. A straightforward calculation using the methods of [10–12] gives

$$\begin{aligned} j &= (\pi/2)e \int {\rm d}\varepsilon\, \chi_\varepsilon \sum_p |t_p|^2 [(2n_p - 1) \\ &\quad \cdot \delta(\varepsilon - \varepsilon_p + eV) - (2n_p - 1) \cdot \delta(\varepsilon - \varepsilon_p)] \\ &= \pi e \int {\rm d}\varepsilon\, \chi_\varepsilon |t_\varepsilon|^2 (n_{\varepsilon - eV} - n_\varepsilon). \end{aligned} \qquad (2)$$

Taking for simplicity $N(\varepsilon) = m/(\pi\hbar^2)$ from equation (2) one finds the zero temperature steady state conductance as

$$G_0 = \frac{e^2}{\hbar^2} \overline{T} W \sqrt{2meV_{\rm sd}} = \frac{2e^2}{h} \overline{T} N_{\rm ch}(V_{\rm sd}) \qquad (3)$$

where $\overline{T} = |t_{eV_{\rm sd}}|^2$ is the graphene barrier transparency. In equation (3) we introduced the voltage-dependent dimensionless number of conducting channels $N_{\rm ch}(V_{\rm sd}) = \pi W \sqrt{2meV_{\rm sd}}$. The dependence $N_{\rm ch}$ versus $V_{\rm sd}$ stems from the energy dependence of the electron velocity in the bilayer graphene v_ε. Equation (3) coincides with the well-known Landauer formula with the number of conducting channels $N_{\rm ch}$. The calculation results will be convenient to normalize to an auxiliary conductivity defined as $\tilde{\sigma}_0 = W^{-1} \cdot G_0(V_{\rm sd} = U_0/e) = (2e^2/h)\pi\sqrt{2mU_0}$ (where we used $\overline{T} \simeq 1$ at $V_{\rm sd} = U_0/e$, U_0 being the graphene barrier height). The transmission amplitude t_ε across the voltage biased junction is obtained within a simple model which represents the chiral fermion wavefunctions via Airy functions. The Hamiltonian (1) yields

a gapless semiconductor with massive chiral electrons and holes having a finite mass m. Let us consider tunneling of those fermions with the energy E incident on the barrier under the angle ϕ. Since the potential barrier is formed in the longitudinal direction, the y component $\hbar q$ of the momentum $\mathbf{p}$ is conserved while the x component $\hbar k$ is not. The trial chiral fermion wavefunction takes a piecewise form [1]. The chirality has no significance for particles propagating above the barrier $E > U_0$. An analytical steady state solution [1] is obtained at $V_{\rm sd} = 0$ for a rectangular barrier expressing the electron and hole wavefunctions via combinations of plane waves. Matching the continuous boundary conditions one finds [1–4] the tunneling amplitude $t_{\rm 2GW}$ for a normal electron incidence ($\phi = 0$) as

$$t_{\rm 2GW} = -\frac{2k(k'-k)s\mathrm{e}^{2\mathrm{i}(Dk'+2\varphi)}}{\mathrm{e}^{2\mathrm{i}Dk'(k-k')^2s'-(k+k')^2s'}} \tag{4}$$

where the electron wavevector in the electrode is $k = \sqrt{2m|E|}/\hbar$ and inside the barrier is $k' = \sqrt{2m(E-U_0)}/\hbar$, φ is the phase drop across the graphene barrier, $s' = \mathrm{sign}(U_0 - E)$. For a classic rectangular barrier one instead obtains

$$t_{\rm cl} = \frac{kk'\mathrm{e}^{-\mathrm{i}Dk}\mathrm{e}^{\mathrm{i}\varphi}}{kk'\cos(Dk') - \mathrm{i}\left(k^2+k'^2\right)\sin(Dk')/2}. \tag{5}$$

Although equations (4) and (5) are instructive, the experimentally measured characteristics are relevant rather to a finite bias voltage ($V_{\rm sd} \neq 0$) across the graphene barrier and finite incidence angles $\phi \neq 0$. The electric field $\mathcal{E}$ in the latter case penetrates inside the bilayer graphene barrier and electrodes, forcing the charge carriers to accelerate. The simplest electron and hole wavefunctions in that case are represented via the Airy functions [13] rather than via plane waves. The CF wavefunction $\hat{\Psi}(x)$ is obtained from the Dirac equation $\hat{H}\hat{\Psi} = E\hat{\Psi}$, where E is the electron energy. For calculations one uses the tilted barrier potential $U(x) = -\mathcal{E}x[\theta(-x) + \theta(x-D)] + [U_0 - \mathcal{E}x]\theta(x)\theta(D-x)$, where $\mathcal{E} = V_{\rm sd}/D$ is the electric field, which penetrates into the graphene barrier. Then components of the fermion momentum $\mathbf{p} = (\hbar k, \hbar q)$ are written as $\hbar q = \sqrt{2m|E|}\sin\phi$ and $\hbar k(x) = \mathrm{i}\sqrt{2m(U(x)-E)}\cos\phi(x)$, $\phi(x) = \arcsin[(q/k(x))\sin\phi]$, where D is the barrier thickness and ϕ is the electron incidence angle in electrode 1. The corresponding trial wavefunction is

$$\begin{aligned}
\hat{\Psi} &= \hat{\Psi}_1\theta(-x) + \hat{\Psi}_2\theta(D-x) + \hat{\Psi}_3\theta(x-D)\\
\hat{\Psi}_1 &= \mathrm{e}^{\mathrm{i}qy}[\lambda\mathrm{Bi}(\zeta_{k,x}) + b_1\tilde{\lambda}\mathrm{Bi}(\zeta_{k,x}) + c_1\lambda^{\dagger}\mathrm{Ai}(\zeta_{ik,x})]\\
\hat{\Psi}_2 &= \mathrm{e}^{\mathrm{i}qy}[a_2\mathrm{Ai}(\zeta_{k',x})\mu + b_2\mathrm{Bi}(\zeta_{k',x})\tilde{\mu}\\
&\quad + d_2\mathrm{Bi}(\zeta_{ik',x})\mu^{\dagger} + c_2\mathrm{Ai}(\zeta_{ik',x})\mu^{\ddagger}]\\
\hat{\Psi}_3 &= \mathrm{e}^{\mathrm{i}qy}[a_3\mathrm{Ai}\left(\zeta_{k,x}\right)\nu + d_3\mathrm{Bi}\left(\zeta_{ik,x}\right)\tilde{\nu}]
\end{aligned} \tag{6}$$

where

$$\zeta_{k,x} = -\left(k^2 + \mathcal{E}x\right)/\left(-\mathcal{E}\right)^{2/3} \tag{7}$$

$k = \sqrt{2m|E|}\cos\phi/\hbar$ is the electron wavevector in the electrode and $k' = \sqrt{2m(E-U_0)}\cos\phi'/\hbar$ is the electron wavevector inside the graphene barrier. In the above formulae we used the following notations:

$$\phi' = \arcsin\left((q/k')\sin\phi\right)$$

$$s_1 = -1, \qquad s_2 = \mathrm{sign}\,(U_0 - E)\,,$$

$$s_3 = \mathrm{sign}\,(-V_{\rm sd} - E)$$

$$h' = \sqrt{1+\sin^2\phi'} - \sin\phi'$$

$$\lambda = (|\uparrow\rangle + s_1\mathrm{e}^{2\mathrm{i}\phi}\,|\downarrow\rangle)$$

$$\tilde{\lambda} = (|\uparrow\rangle + s_1\mathrm{e}^{-2\mathrm{i}\phi}\,|\downarrow\rangle)$$

$$\lambda^{\dagger} = (|\uparrow\rangle + s_1h_1\,|\downarrow\rangle)$$

$$\nu = \left(|\uparrow\rangle + s_3\mathrm{e}^{2\mathrm{i}\phi}\,|\downarrow\rangle\right)$$

$$\tilde{\nu} = (|\uparrow\rangle - s_3/h_3\,|\downarrow\rangle)$$

$$\mu = (|\uparrow\rangle + s_2\mathrm{e}^{2\mathrm{i}\phi'}\,|\downarrow\rangle)$$

$$\tilde{\mu} = (|\uparrow\rangle + s_2\mathrm{e}^{-2i\phi'}\,|\downarrow\rangle)$$

$$\mu^{\dagger} = (|\uparrow\rangle - s_2/h_2\,|\downarrow\rangle)$$

$$\mu^{\ddagger} = (|\uparrow\rangle - s_2h_2\,|\downarrow\rangle).$$

In the above equations we introduced auxiliary matrices $|\uparrow\rangle^{\rm T} = \begin{pmatrix}1 & 0\end{pmatrix}$ and $|\downarrow\rangle^{\rm T} = \begin{pmatrix}0 & 1\end{pmatrix}$ (where T means transpose). The chiral tunneling is pronounced at finite incidence angles $\phi \neq 0$ and at energies $E < U_0$ below the barrier. The steady state tunneling probability T_0 of a normally incident chiral particle vanishes below the barrier ($E < U_0$) while it is finite above the barrier (when $E \geqslant U_0$). In figure 2(a) we plot T_0 versus the energy E of an electron incident on the barrier under the angle ϕ. In figure 2(b) we show the steady state tunneling differential conductance $\sigma_0(V_{\rm sd})$ for different incidence angles ϕ. Both the plots in figures 2(a) and (b) are related to $U_0 = 2$ meV, which

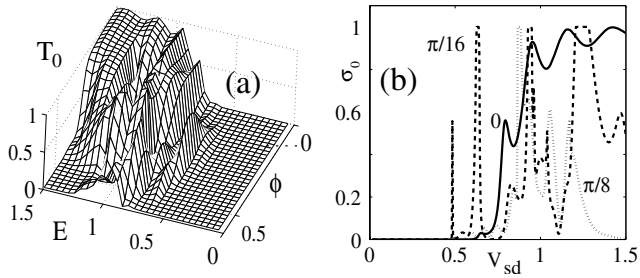

Figure 2. (a) The steady state tunneling transparency T_0 versus the electron energy E (in units of the graphene barrier height U_0) and the azimuthal angle ϕ (in radians). (b) The corresponding steady state differential conductance σ_0 (in units of $\tilde{\sigma}_0 = (2e^2/h)\pi\sqrt{2mU_0}$) versus the source–drain bias voltage $V_{\rm sd}$ (in units of U_0/e) for three angles of incidence ϕ. The sharp peaks at $V_{\rm sd} < U_0/e$, when $\phi \neq 0$, originate from the electron–hole interference inside the barrier.

corresponds to the surface charge density $n = 10^{11}$ cm^{-2} induced by the gate voltage $V_G = 1$ V across the SiO_2 substrate with thickness $d = 300$ nm (see figures 1(c) and (d)).

3. Directional photoelectric current

The steady state characteristics of the dc biased graphene junction described above allow study of the external ac field influence on the graphene junction. We find that a most spectacular phenomenon occurs when the ac gate voltage $V_G(t)$ modulates the height U of the graphene barrier $U \to U_0 + U_1 \cos \Omega t$, where Ω is the ac field frequency. Then the $\hat{x}$ component of the electron momentum $\hbar k_B = \sqrt{2m(U_0 - E)} \cos \phi'$ inside the barrier becomes time-dependent $k_B \to k_B + \kappa(t)$ which, at $\kappa(t) \ll k_B$, gives $\kappa(t) = (U_1/2k_B) \cos \Omega t + (U_1^2/8k_B^3) \cos^2 \Omega t + O(U_1)$. We emphasize that a mere factorization [5] of the electron wavefunction $\hat{\Psi}(x,t)$ like $\hat{\Psi}(x,t) \to \hat{\Psi}(x) \sum_k J_k(\alpha) \exp(in\Omega t)$ (where $\alpha = eU_1/(\hbar\Omega)$) does not work here since it does not properly incorporate the non-stationary behavior of $\hat{\Psi}(x,t)$. The puzzle comes from a non-analytical dependence of $\hat{\Psi}(x,t)$ on $\kappa(t)$. Therefore one should obtain a valid $\hat{\Psi}(x,t)$ from corresponding non-stationary boundary conditions at the electrode/barrier interfaces. This gives a complex non-stationary and nonlinear behavior of $\hat{\Psi}(x,t)$, from which one computes the observable characteristics of interest. The ac-field-induced time dependence $\kappa(t)$ yields two spectacular consequences. First, the ac field splits the sharp resonance in the energy-dependent transmission probability $\overline{T}(E)$ at $E = E_0$ as $E_0 \to E_0 \pm n\Omega$, where n is the number of photons absorbed during the chiral tunneling process. And, second, the ac field strongly affects the angular dependence of the chiral tunneling since it renormalizes the angle ϕ' between q and $k_B(t)$ inside the barrier as

$$\phi' = \arcsin\left[\left(\overline{q \cdot k_B^{-1}(t)}^{t}\right) \sin\phi\right]. \tag{8}$$

In order to compute the time-dependent electric current one solves the non-stationary boundary conditions. In this way one finds the transmission coefficient $t_E(t)$. Analytical expressions for $t_E(t)$ are obtained in a simplest case $U_0 = 0$ (no graphene barrier when the ac field is off). After the ac field is on, it induces an oscillating potential barrier $U(t) = U_1 \cos \Omega t$ via an ac gate voltage $V_G(t) = V_G^{(0)} \cos \Omega t$. Assuming a normal incidence ($\phi = 0$) and setting $U_0 = 0$, $k_2 = k_1 + \kappa_1$, where κ_1 is time-dependent, one gets

$$t_{E<U_0}(\phi = 0) = \frac{4ik_1k_+(\cosh D\kappa_- + \sinh D\kappa_-)}{4ik_1k_+ \cosh Dk_+ + 2k_1^2 \sinh Dk_+ - 2k_+^2 \sinh Dk_+} \tag{9}$$

where $\kappa_- = \kappa_1 - ik_1$, $k_+ = k_1 + \kappa_1$. Equation (9) corresponds to a set-up where the graphene barrier is induced purely by the ac gate voltage. In the limit of small external ac field ($\kappa_1 \ll k_1$) from equation (9) one obtains

$$\begin{aligned} t_{E<U_0}(\phi = 0) &= 2\mathcal{K}_1 + 2(Dk_1 + i)(1 - e^{2k_1}) \\ &\cdot \mathcal{K}_2\varkappa + (D^2e^{4Dk_1}k_1^2 + D^2k_1^2 - 12iDe^{2Dk_1}k_1 \\ &- 6D^2e^{2Dk_1}k_1^2 + 2iDe^{4Dk_1}k_1 + 2iDk_1 \\ &+ 4e^{2Dk_1} - (2+i) - (2-i)e^{4Dk_1})\mathcal{K}_3\varkappa^2 + O(\kappa_1^3) \end{aligned} \tag{10}$$

where $\varkappa = \kappa_1(t)/k_1$ and we introduced the auxiliary function $\mathcal{K}_p = e^{(1-i)Dk_1}/(1 + e^{2Dk_1})^p$. The transmission resonances correspond to a vanishing denominator $(1 + e^{2Dk_1})^p = 0$, $p = \overline{1 \ldots 3}$. The Fourier transform of the above equation shows that the ac field splits the kth chiral tunneling resonance as $E_k \to E_k \pm n\hbar\Omega$, where n is the number of photons absorbed (emitted) during the tunneling. One can see that the external field not only splits the resonances, but also strongly affects angular dependence of the chiral tunneling. That happens because the ac field causes no influence on the $\hat{y}$ component of the electron momentum q since the graphene barrier is effectively one-dimensional. The time dependence $\kappa_1(t)$ also takes place when the ac field modulates the graphene barrier width as $D \to D_0 + D_1 \cos \Omega t$. Splitting of the chiral tunneling resonances and the angular redistribution of the electric current under the ac field influence is better pronounced for a finite barrier height $U_0 \neq 0$ and $U = U_0 + U_1 \cos \Omega t$. From equation (8) one can see that $\phi' = 0$ if $\phi = 0$. However, if $\phi \neq 0$, one may observe a spectacular phenomena. In this case an external ac field induces a finite electric current for an almost normal incidence $\phi \approx 0$, which was inhibited when the field was off. When $\phi \approx 0$, the ac field actually causes additional photon-assisted chiral tunneling resonances to engage. The directional photoelectric effect (DPE) may be realized in two scenarios. *One scenario* assumes that an electron beam having a finite angular width $\delta\phi \neq 0$ enters the graphene barrier normally. A visible DPE can be achieved in the set-up shown in figure 4(b) where the attached electrodes 1 and 3 are made of one-dimensional conducting wires. If the wire is much narrower than the width of the graphene stripe ($W_w \ll W$), one may consider the electric current as a result of one-dimensional propagation of an electron along the trajectories under the influence of the bias voltage. Such a method formerly had intensively been used in numerous works devoted to point contact junctions [14, 15]. If the electric current is sufficiently weak, the electrons coming from the wire into the graphene stripe introduce a negligible disturbance into the electron spectrum inside the graphene. The translational invariance inside graphene is well preserved [16]. The authors of [16] used the STM tip for imaging the electron wavefunction in carbon nanotubes which showed a periodic pattern. Electrode 1 emits electrons under a small but finite angle ϕ ($\phi \ll \pi$, $\phi \neq 0$) whose trajectories are focused/defocused by the external electromagnetic field as indicated in figure 4(b). The frequency dependence of the transparency is governed by the directional photoelectric effect. A significant directional photoelectric effect emerges even for a relatively long wavelength $\lambda \simeq 1$ mm–0.01 μm (which corresponds to the THz domain) if the condition $|E - U_0 \mp \Omega| \ll |E|$ is met. The deviation angle $\phi' = \arcsin[\sqrt{|E|/|E - U_0 \mp \Omega|} \sin\phi]$ inside the graphene barrier considerably increases, giving $\phi' \gg \phi$. This means that an ideal transparency taking place in the steady state at $\phi \neq 0$ is redistributed over the angle ϕ' after the ac field is applied. The transparency peaks are actually shifted from finite angles $\phi \neq 0$ to the normal incidence angle $\phi = 0$. *Another scenario* involves an incident single electron which enters the graphene barrier strictly normally ($\phi = 0$) under the influence of a high frequency THz wave. In this scenario

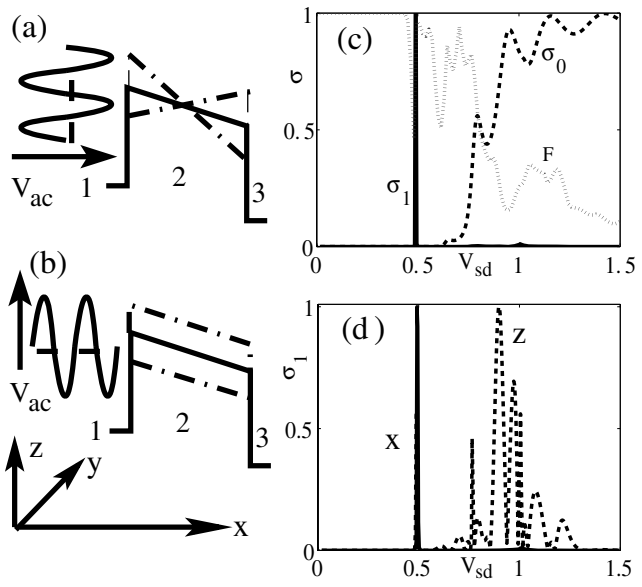

Figure 3. Limit of a low ac field amplitude. Photoelectric effect in the bilayer graphene junction induced by an external electromagnetic field. Modulation of the graphene barrier height by the ac field polarized along $\hat{x}$ (a) and $\hat{z}$ (b) axes. The dashed–dotted lines in (a) and (b) show deviations of the chiral barrier $U(x)$ from its steady state shape under influence of the ac field $V_{\rm ac}$. (c) Corresponding steady state σ_0 and the photon-assisted chiral tunneling differential $\sigma_1 = \overline{\sigma^t} - \sigma_0$ conductances (same units as in figure 2(b)) in the longitudinal direction $\phi = 0$. Curve F shows the Fano factor F, which characterizes the Poisson noise. (c) The dc conductance for $\hat{x}$ and $\hat{z}$ field polarizations. One may notice that the ac field induces sharp resonant peaks in the photon-assisted chiral tunneling conductance σ_1.

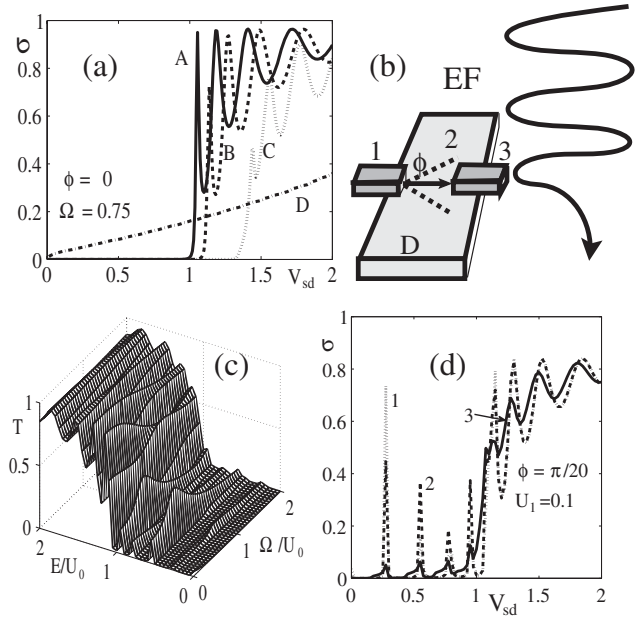

Figure 4. The time-averaged differential conductance $\overline{\sigma(t)}^t$ (in units of $\tilde{\sigma}_0 = (2e^2/h)\pi\sqrt{2mU_0}$) of a bilayer graphene junction exposed to an external electromagnetic field which modulates the barrier height $U(t) = U_0 + U_1 \cos\Omega t$. In figure (c) one may notice a remarkably strong DPE at $\Omega/U_0 \simeq 1$. This corresponds to curve 1 in figure (d) where the peak spacing Δ_k is determined by the graphene barrier length D.

an electron absorbs a THz photon having the finite energy E_Ω and momentum q along the y axis. Then the electron deviation angle $\delta\phi$ just before entering the barrier is small, $\delta\phi \ll \pi$. For instance, taking $\nu = 30$ THz (which corresponds to the photon energy $E_\Omega = 125 \times 10^{-3}$ eV) one gets $\delta\phi \approx q/k = 2 \times 10^{-3}$. The photoelectric effect is well pronounced for an electron with energy $E_{\rm e} \simeq 2 \times 10^{-3}$ eV after it gets inside the graphene barrier. There, if $|E - U_0 \mp \Omega| \ll |E|$ the deviation angle $\phi' = \arcsin[\sqrt{|E|/|E - U_0 \mp \Omega|}\sin\phi]$ increases considerably, since the photon energy is pretty high, $E_\Omega/E_{\rm e} \simeq 50$, $E_\Omega = 0.1$ eV. Practically this means that one must set $\hbar\Omega \simeq U_0$ to get a strong photoelectric effect. In the above example the last condition also supposes that one should use $U_0 \approx E_\Omega = 125$ meV. Below we consider the two most important field polarizations along the $\hat{x}$ and $\hat{z}$ axes as shown in figures 3(a) and (b). The barrier transparency $T(E, \phi)$ is affected by the ac field directly in either case. In particular, the barrier shape is modulated by the ac field polarized along the x direction as sketched in figure 3(a), since $\mathcal{E} \to \mathcal{E}_0 + \mathcal{E}_1 \cos(\Omega t)$. On the other hand, if one applies an ac field polarized as $\mathbf{E} = (0, 0, E_z)$, it modulates the barrier height since $V_{\rm G} \to V_{\rm G}^{(0)} + V_{\rm G}^{(1)} \cos(\Omega t)$ ($V_{\rm G}^{(0)}$ is the steady state gate voltage and $V_{\rm G}^{(1)}$ is the ac-field-induced addition, see sketch in figure 3(b)). Then the ac-field-induced correction to the dc tunneling current is $j_1 = 2e \int {\rm d}\varepsilon\, \chi_\varepsilon |\delta t^{(1)}_{\varepsilon,\Omega}|^2 (2n_\varepsilon - n_{\varepsilon+\Omega-eV} - n_{\varepsilon-\Omega-eV})$, where the transmission amplitude $t^{(1)}_{\varepsilon,\Omega}$ is obtained from the corresponding non-stationary boundary conditions at $x = 0$ and D. Physically, the directional photoelectric effect (DPE) comes from an ingenious influence of the external electromagnetic field on the electron–hole phase correlations during the chiral tunneling. Technically, modulation of the barrier height by the ac field shifts positions of the sharp peaks in the energy-dependent barrier transparency $\overline{T}(\varepsilon \pm \Omega)$. Besides, it also modifies the overall angular distribution of the electric current, so the electron–hole conversions occur with an additional phase shift. Numerical results for both cases are presented in figures 3(c) and (d). Corresponding plots for the steady state differential conductance $\sigma_0(V_{\rm sd})$ and for the photon-assisted chiral tunneling conductance $\sigma_1(V_{\rm sd}) = \partial j_1/\partial V_{\rm sd} = \overline{\sigma^t} - \sigma_0$ both indicate the angular redistribution of the photon-assisted chiral tunneling current across the graphene barrier. The steady state conductance curve σ_0 in figure 3(c) corresponds to $U_0 = 2$ meV while curve σ_1 is computed for $V_{\rm G} = 1$ V and $\Omega = 1$ THz. The DPE is well illustrated by the sharp scattering resonance taking place in $\sigma_1(V_{\rm sd})$ (see the crisp peak at the incidence angle $\phi = \pi/16$ and at the bias voltage $V_{\rm sd} = U_0 = 0.5$ in figure 3 (c)). When the ac field is off, the steady state tunneling at $V_0 = 0.5$ in the straightforward direction is suppressed (see the corresponding curve $\sigma_0(V_{\rm sd})$ for $\phi = 0$). However, if one applies the ac field with frequency Ω and $\mathbf{E} = (E_x, 0, 0)$, it opens tunneling channels in the straightforward direction $\phi = 0$, as is evident from curve σ_1 in figures 3(c). In figure 3(d) we compare two time-averaged conductance curves $\sigma_1(V_{\rm sd})$ under the influence of

the ac field with two different polarizations along the $\hat{x}$ (curve X) and $\hat{z}$ (curve Z) axes correspondingly. In either case the $\sigma_1(V_{sd})$ curves show remarkable sharp peaks, whose position, however, changes versus the field polarization. Although the above results are illustrative, they focus solely on the limit of a weak electromagnetic field $U_1 \ll U_0$. Influence of an external electromagnetic field of arbitrary amplitude on the ac transport properties of a bilayer graphene junction had been studied in this work using a numerical approach. We solved the non-stationary boundary conditions using the trial function (6) where we take $\mathcal{E} \rightarrow \mathcal{E}_0 + \mathcal{E}_1 \cos(\Omega t)$ with an arbitrary ratio $\mathcal{E}_1/\mathcal{E}_0$. We emphasize again that a mere multiphoton approximation like that used in [5] is not working in this case. The graphene barrier transparency now is not assumed to be small, therefore the electron wavefunction cannot be simply factorized as $\hat{\Psi}(x,t) \rightarrow \hat{\Psi}(x)\sum_k J_k(\alpha)\exp(\mathrm{i}k\Omega t)$. Therefore we use a straightforward numerical solution of the non-stationary boundary conditions for $\hat{\Psi}(x,t)$ and compute the time-dependent transmission probability $T(t)$ directly from that solution. Then we apply a fast Fourier transform algorithm for computing $\overline{T}(\omega)$ numerically versus the external field frequency Ω and the ac barrier amplitude U_1. The obtained results for the differential conductance under the influence of a strong electromagnetic field with $\Omega/U_0 = 0.75$ are presented in figure 4. In figure 4(a) we show the time-averaged conductance $\overline{\sigma} = \overline{\sigma(t)}^t$ of the bilayer graphene junction for the normal electron incidence $\phi = 0$ and for different ac field amplitudes $U_1 = 0.01$ (curve A), $U_1 = 0.1$ (curve B), $U_1 = 0.4$ (curve C) and $U_1 = 1.3$ (curve D). One can see that, if the external field amplitude U_1 is lower than the graphene barrier height $U_1 < U_0$ (which corresponds to curves A–C), the junction's conductance has a threshold character versus the bias voltage V_{sd}. If, however, $U_1 > U_0$, a finite transparency takes place even at $V_{sd} < U_0$, which corresponds to curve D. From the three-dimensional plot $T_0(\varepsilon, \Omega)$ shown in figure 4(c) one can see that a visible transparency is achieved at frequencies $\Omega/U_0 \approx 1$, which is well consistent with the semi-qualitative consideration above. A more accurate estimation of the DPE magnitude follows from figure 4(d) where we plot $\overline{\sigma}(V_{sd})$ for three different frequencies $\Omega/U_0 = 1$ (curve 1), $\Omega/U_0 = 0.1$ (curve 2) and $\Omega/U_0 = 2$ (curve 3). The peaks of finite $\overline{\sigma}$ in curves 1–3 at $E_k < U_0$ are present because the electron incidence angle ϕ is finite though small ($\phi = \pi/20$). The peak increase of the junction's conductance $\sigma(V_{sd}^{(k)})$ is achieved at selected bias voltage values $V_{sd}^{(k)} < U_0/e$ and $\Omega/U_0 \approx 1$, which corresponds to curve 1. One can see that the directional photoelectric effect increases the junction conductance $\sigma(V_{sd}^{(k)})$ at $\Omega/U_0 \approx 1$ by a few orders of magnitude as compared to its steady state value at the same $V_{sd}^{(k)}$. The relevant increase of the conductance is, however, less significant at other ac field frequencies, i.e. $\Omega/U_0 = 0.1$ (curve 2) and $\Omega/U_0 = 2$ (curve 3). In figures 5(a) and (b) we show contour plots of the time-averaged conductance $\overline{\sigma(t)}^t$ of a bilayer graphene junction versus the electron incidence angle ϕ and the source–drain bias voltage V_{sd} for two different ac field frequencies (a) $\Omega/U_0 \simeq 0.1$ and (b) $\Omega/U_0 \simeq 1$. The conductance diagrams in either case have pretty spectacular complex structures where the dark spots

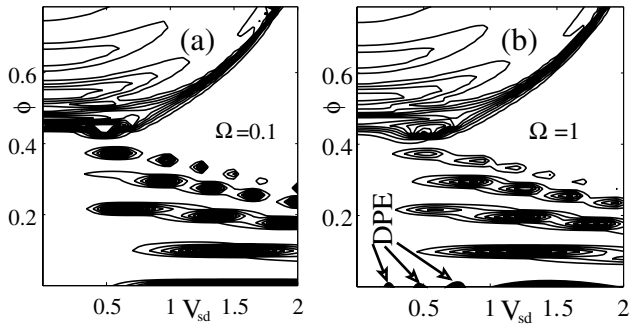

Figure 5. Contour plots of the time-averaged differential conductance $\overline{\sigma(t)}^t$ (in units of $\tilde{\sigma}_0$) of a bilayer graphene junction versus V_{sd} and ϕ at two different ac field frequencies (a) $\Omega/U_0 \simeq 0.1$ and (b) $\Omega/U_0 \simeq 1$.

correspond to $\overline{\sigma}^t \simeq \tilde{\sigma}_0$. When the external field frequency Ω is low (i.e. $\Omega/U_0 = 0.1$, as shown in figure 5(a)), the tunneling for the incident electron energies $E/U_0 < 0.55$ is fully blocked. However, when the field frequency becomes higher, i.e. $\Omega/U_0 = 1$, as indicated in figure 5(b), one may notice a series of sharp dark spots at discrete energies E_k below the barrier ($E_k < U_0$) pronounced at the normal incidence angle $\phi = 0$. Those dark spots constitute the directional photoelectric effect discussed above and indicated as DPE in figure 5(b).

Intrinsic noise in the bilayer graphene junction originates as follows. The thermal noise comes from phonons emitted in the electron–phonon collisions. The matrix element of the electron–phonon collisions according to [17, 18] is $M_{pp'} \propto \langle p|M(x)|p'\rangle \cos(\phi_{pp'})$, where $\phi_{pp'}$ is the angle between initial and final states. The phase factor $\cos\phi_{pp'}$ plays quite a different role in the bilayer graphene compared to the single-layer graphene [17] where it is rather $\cos(\phi_{pp'}/2)$ instead. In the latter case, the factor ensures suppression of the electron–phonon and electron–impurity collisions and the transport of the change carriers remains ballistic up to room temperatures. In contrast, thermal noise in the bilayer graphene devices is rather high at room temperature. Another intrinsic noise (Poisson noise) arises due to the 'Zitterbewegung' effect, which is linked to a jittering motion of the change carriers when electrons are randomly converted back and forth to holes. That produces noise even in the zero temperature limit. The noise is characterized by the Fano factor $F = \sum_n T_n(1-T_n)/\sum_n T_n$, where T_n is the tunneling probability in the nth channel and the summation is performed over all the conducting channels (in our set-up this means just integration over ϕ). From the plot $F(V_{sd})$ shown in figure 3(d) for $D = 15$ (in units of $h/\sqrt{2mU_0}$) one infers that the Poisson noise becomes extremally low at $V_{sd} \geqslant U_0$.

4. Conclusions

In conclusion we computed the electric current across the bilayer graphene junction in conditions when an external electromagnetic field is applied. We have found that the threshold absorption of the external electromagnetic field

strongly depends on the ac field frequency and amplitude. The electromagnetic field induces an ideal transparency of the graphene barrier in the longitudinal direction, which had been fully suppressed when the ac field was off. That directional photoelectric effect originates from an angular redistribution of the whole transparency diagram since the sidebands at finite angles are redirected to the normal incidence. An experimental observation of such a spectacular directional optoelectric phenomena would provide strong evidence for the existence of massive chiral fermions in the bilayer graphene. We emphasize that the threshold absorption emerges purely from a quantum mechanical phase shift, and not from an inelastic excitation by the ac field. That means no heating is involved during the absorption. The ac current induced by the electromagnetic field across the graphene junction has a sharp angular dependence, which potentially can be exploited in sensor nanodevices of the external electromagnetic field. The directional photoelectric effect in the double-layer graphene junctions is a unique phenomenon which exists in that system and had not been noticed in other systems, like junctions composed of single-layer graphene or of normal metals. The most intriguing feature is the switch between zero and finite conductance occurring without energy absorption. The phenomena considered above have a great potential for various nanoelectronic applications.

Acknowledgments

I wish to thank V Chandrasekhar and P Barbara for fruitful discussions. This work had been supported by AFOSR grant FA9550-06-1-0366.

References

[1] Katsnelson M I, Novoselov K S and Geim A K 2006 *Nat. Phys.* **2** 620
[2] Novoselov K S, McCann E, Morozov S, Falko V I, Katsnelson M I, Zeitler U, Jiang D, Schedin F and Geim A K 2006 *Nat. Phys.* **2** 177
[3] McCann E and Falko V I 2006 *Phys. Rev. Lett.* **96** 086805
[4] Nilsson J, Castro Neto A H, Guinea F and Peres N M R 2007 *Phys. Rev.* B **76** 165416
[5] Shafranjuk S E 2007 *Phys. Rev.* B **76** 085317
[6] Foa Torres L E F 2005 *Phys. Rev.* B **72** 245339
Foa Torres L E F and Cuniberti G 2008 arXiv:0807.4953v2 unpublished
[7] Strange P 1998 *Relativistic Quantum Mechanics* (Cambridge: Cambridge University Press)
[8] Krekora P, Su Q and Grobe R 2004 *Phys. Rev. Lett.* **92** 040406
[9] Novoselov K S, Geim A K, Morozov S V, Jiang D, Zhang Y, Dubonos S V, Grigorieva I V and Firsov A A 2004 *Science* **306** 666
[10] Yeyati A L and Büttiker M 1995 *Phys. Rev.* B **52** R14360
[11] Keldysh L V 1965 *Sov. Phys.—JETP* **20** 1018
[12] Datta S 1997 *Electronic Transport in Mesoscopic Systems* (Cambridge: Cambridge University Press)
[13] Korn G A and Korn T M 1967 *Handbook for Scientists and Engineers* (New York: McGraw-Hill)
[14] Yanson I K 1974 *Zh. Eksp. Teor. Fiz.* **66** 1035
Yanson I K 1974 *Sov. Phys.—JETP* **39** 506 (Engl. Transl.)
[15] Shekhter R I and Kulik I O 1983 *Fiz. Nizk. Temp.* **9** 46
Shekhter R I and Kulik I O 1983 *Sov. J. Low Temp. Phys.* **9** 22 (Engl. Transl.)
[16] Venema L C, Wildöer J W G, Janssen J W, Tans S J, Temminck Tuinstra H L J, Kouwenhoven L P and Dekker C 1999 *Science* **283** 52
[17] Ando T, Nakanishi T and Saito R 1998 *J. Phys. Soc. Japan* **67** 2857
Ando T and Nakanishi T 1998 *J. Phys. Soc. Japan* **67** 1704
[18] McEuen P L, Bockrath M, Cobden D H, Yoon Y G and Louie S 1999 *Phys. Rev. Lett.* **83** 5098